Supplement of The Cryosphere, 20, 4877–4910, 2026
https://doi.org/10.5194/tc-20-4877-2026-supplement
© Author(s) 2026. CC BY 4.0 License.

The Cryosphere Open Access EGU

Supplement of

The missing drifts: snow density heterogeneity from wind-packing exacerbates systematic underestimation of deep snow storage from the scale of nivation hollows to mountain ranges

Elijah N. Boardman et al.

Correspondence to: Elijah N. Boardman (eli.boardman@mountainhydrology.com)

The copyright of individual parts of the supplement might differ from the article licence.

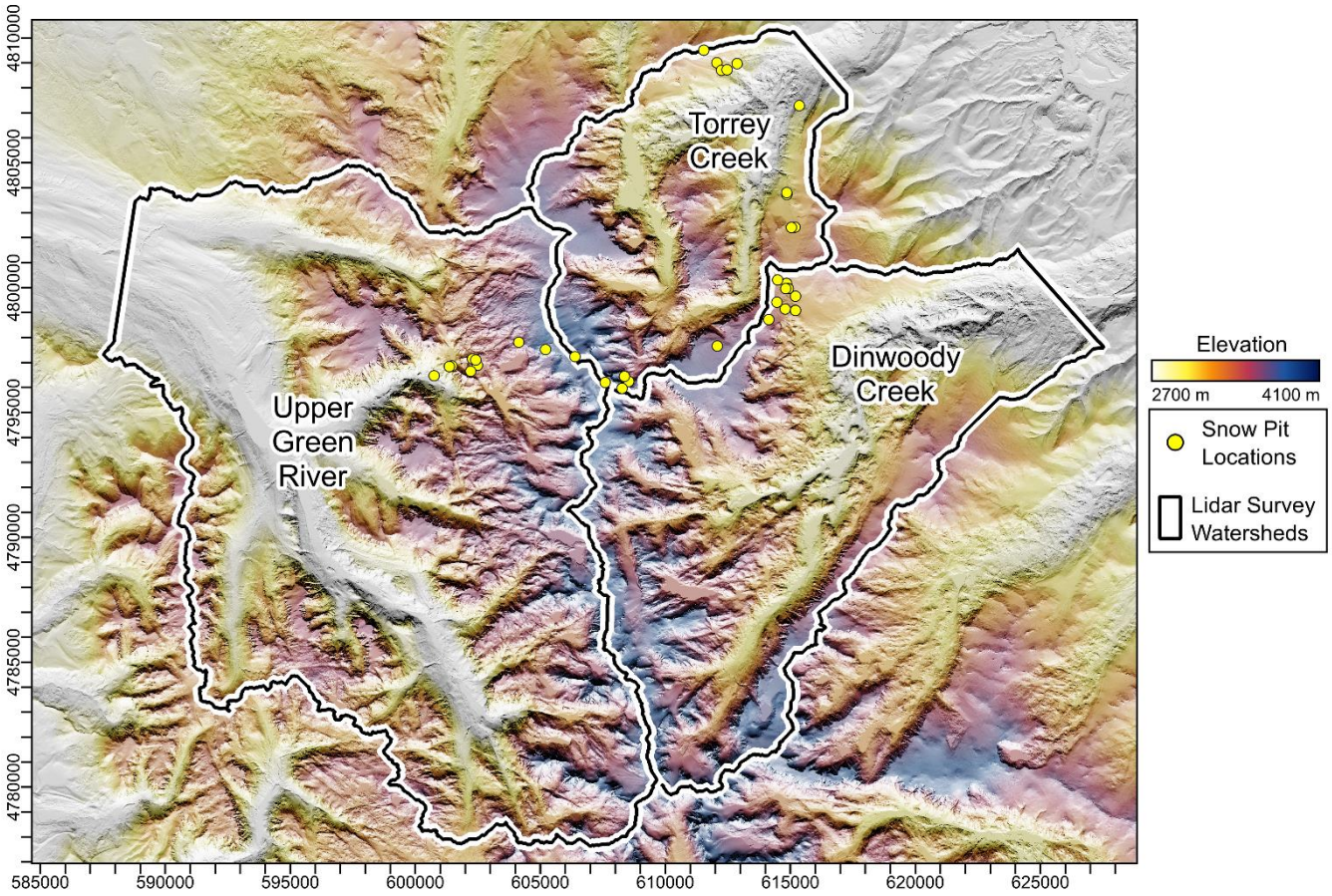

Figure S1: Maps of the three lidar-surveyed watershed areas considered in this study: Torrey Creek (121 km^2), Dinwoody Creek (219 km^2), and the upper Green River (391 km^2).

5

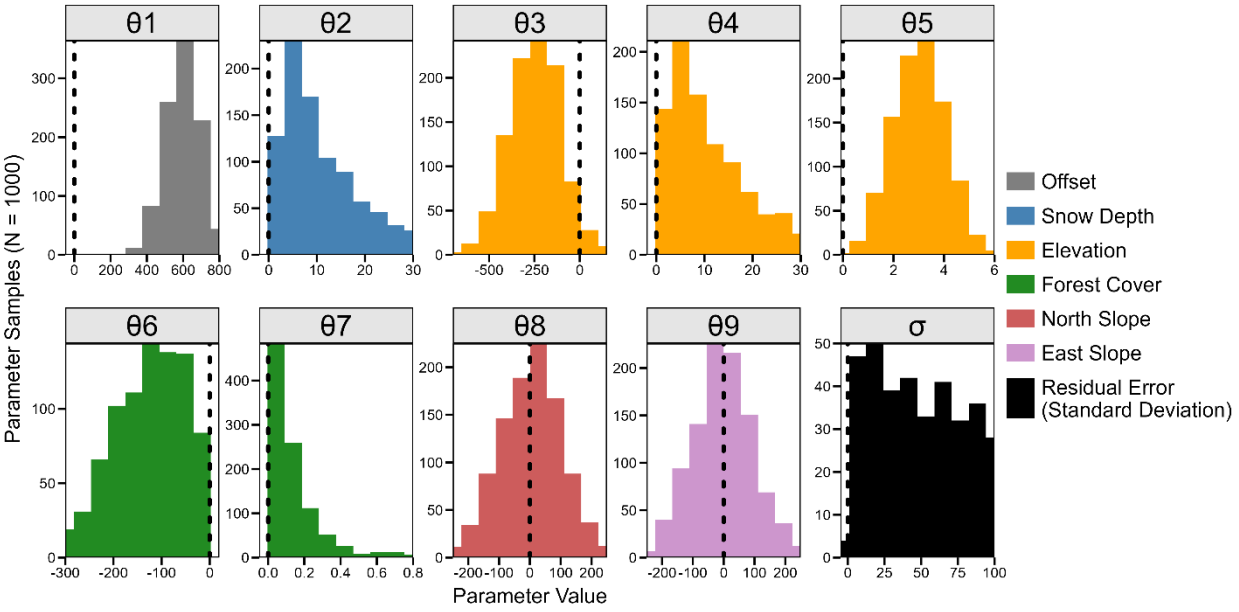

Figure S2: Prior parameter distributions for the Bayesian regression model (Eq. 1), specified as follows: θ1~normal(600, 100); θ2~lognormal(log(10), 1); θ3~normal(-250, 100); θ4~lognormal(log(10), 1); θ5~normal(3, 1); θ6~normal(-100, 100)T[,0]; θ7~lognormal(log(0.1), 1)T[0.01,]; θ8~normal(0, 100); θ9~normal(0, 100); σ~normal(0, 100)T[0,]. The notation T[lower,upper] indicates that the distribution is truncated at the specified lower or upper bound.

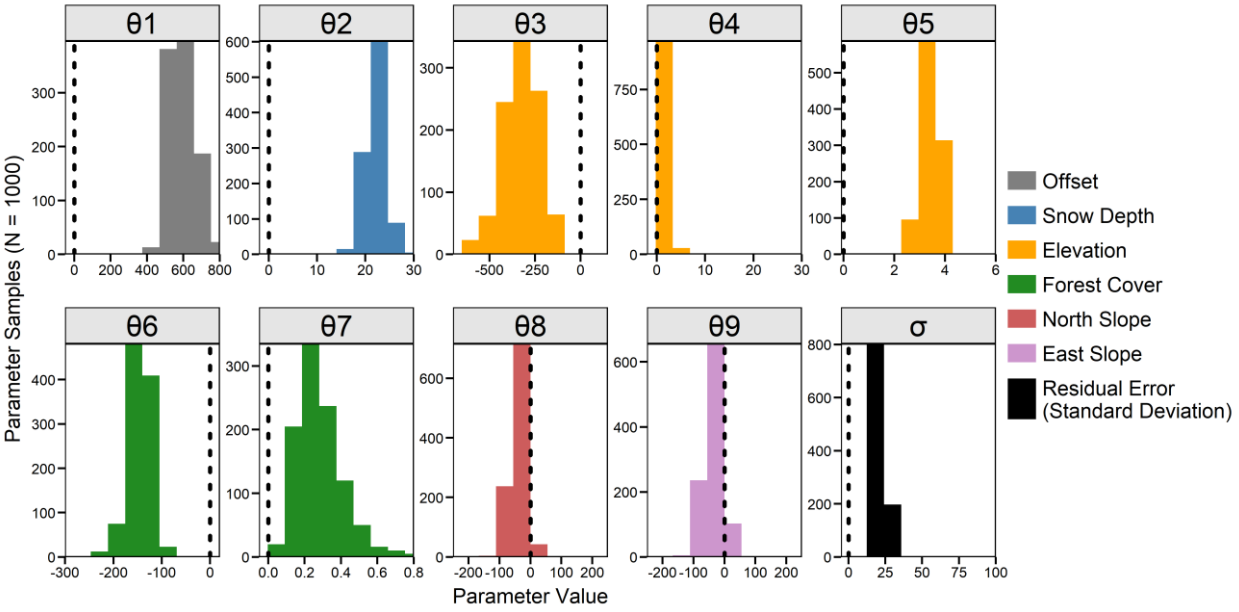

Figure S3: Posterior parameter distributions after sampling the Bayesian regression model (Eq. 1) using the snow pit data. Note that Figs. S1-S2 have the same horizontal axes scales for each parameter, showing the shift in distributions and reduction in parameter uncertainty.

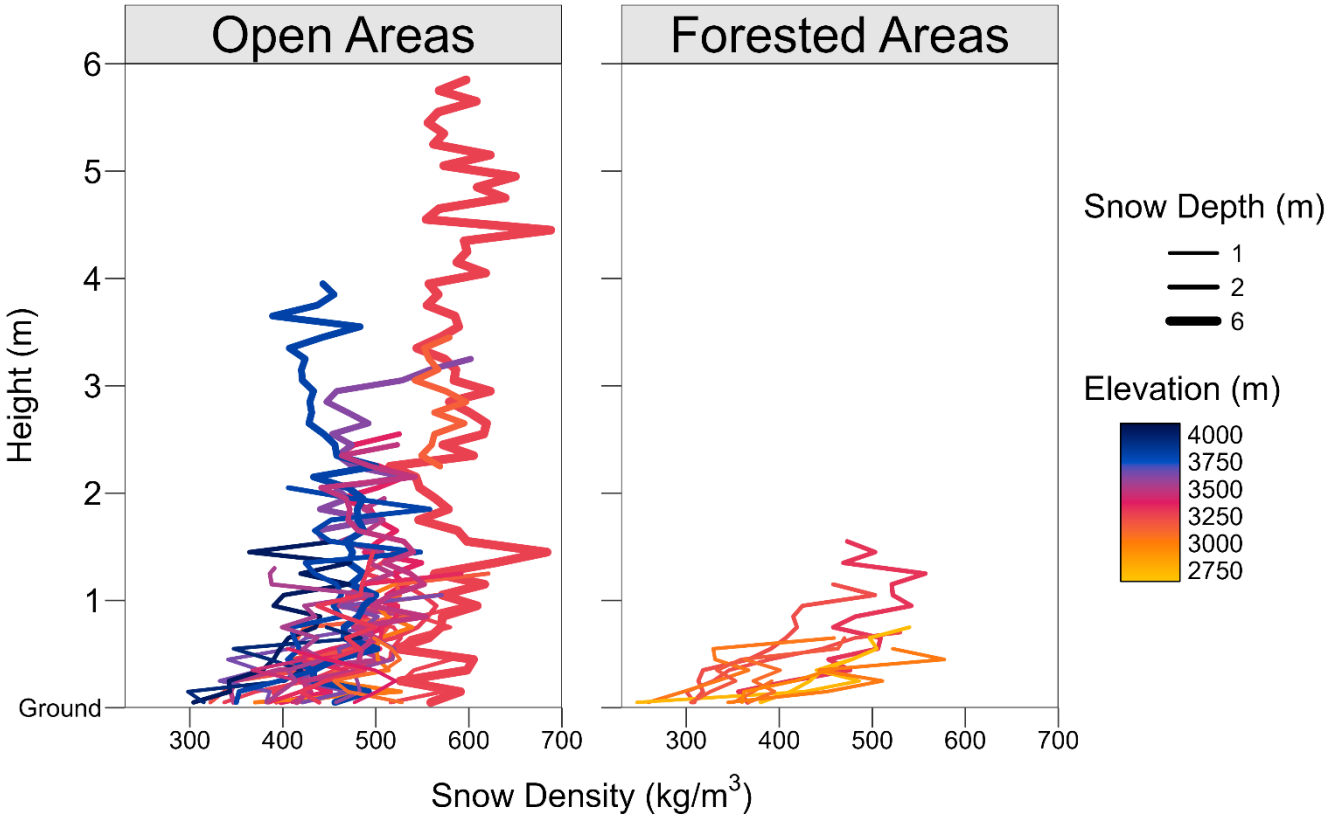

Figure S4: Vertical snow density profiles from the 36 snow pits collected in 2025 (subset of Fig. 2 in the main manuscript).

Figure S5: Overview photograph of the Burrow Flat (foreground) and Downs Mountain (distant) region (cf. Fig. 1), captured August 23, 2023. Small portions of the Burrow Flat drift continue to persist at this point in the late summer. Lighter-colored soil provides evidence of accelerated chemical weathering in the topographic concavity formed by the nivation hollow. A darker green region of alpine willows (Salix spp.) and other meadow vegetation extends from the base of the drift, apparently subsidized by meltwater from this location. The prevailing wind vector points out of the page (the camera is looking upwind).

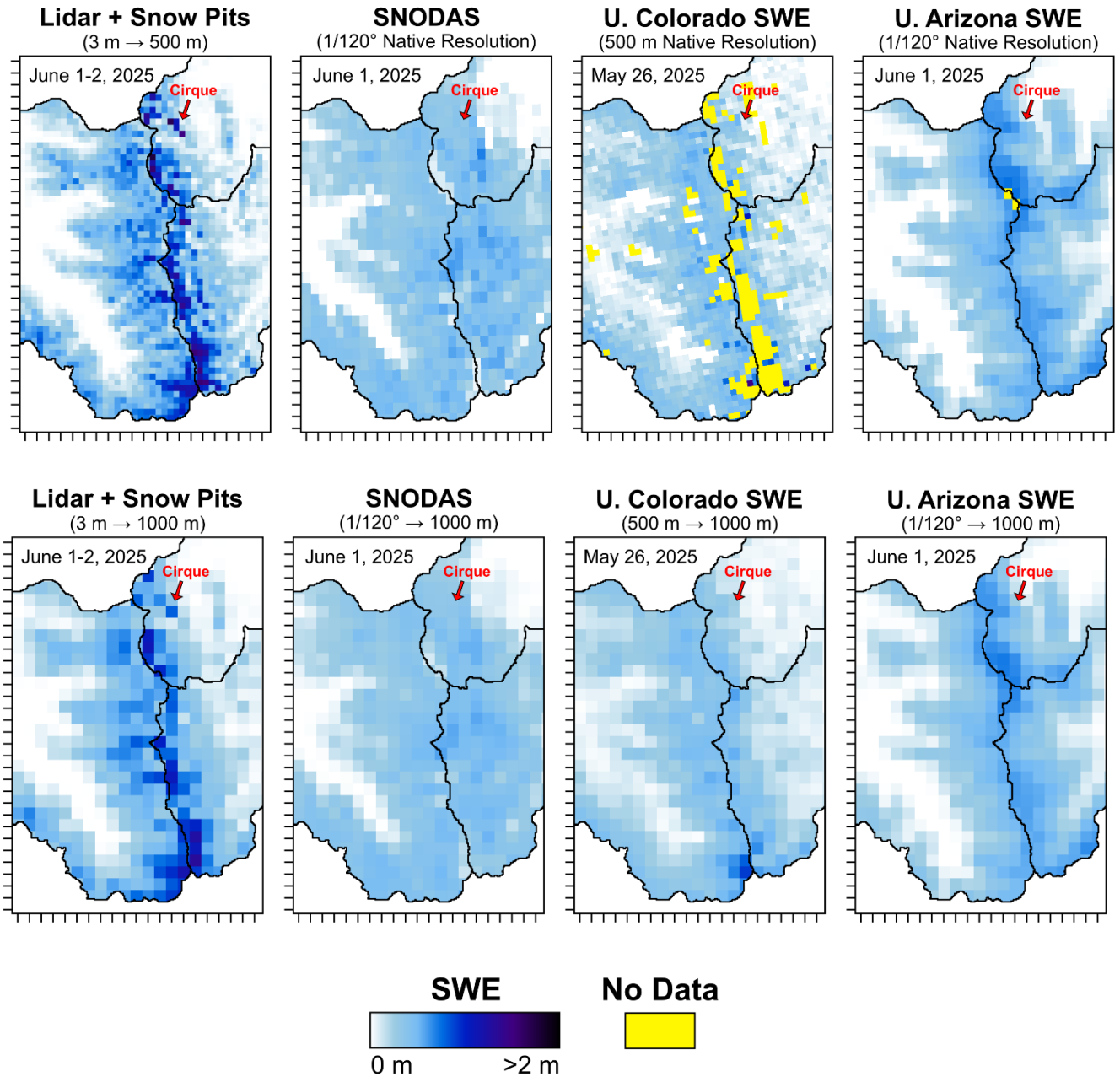

Figure S6: Comparison of SWE heterogeneity analogous to Fig. 10 in the manuscript. The top row of panels shows the native resolution for each of the non-lidar datasets, including missing values (yellow pixels) in the U. Colorado and U. Arizona products. The bottom row of panels compares the same datasets after interpolating missing data and aggregating all datasets to the same 1000 m grid resolution and UTM projection.

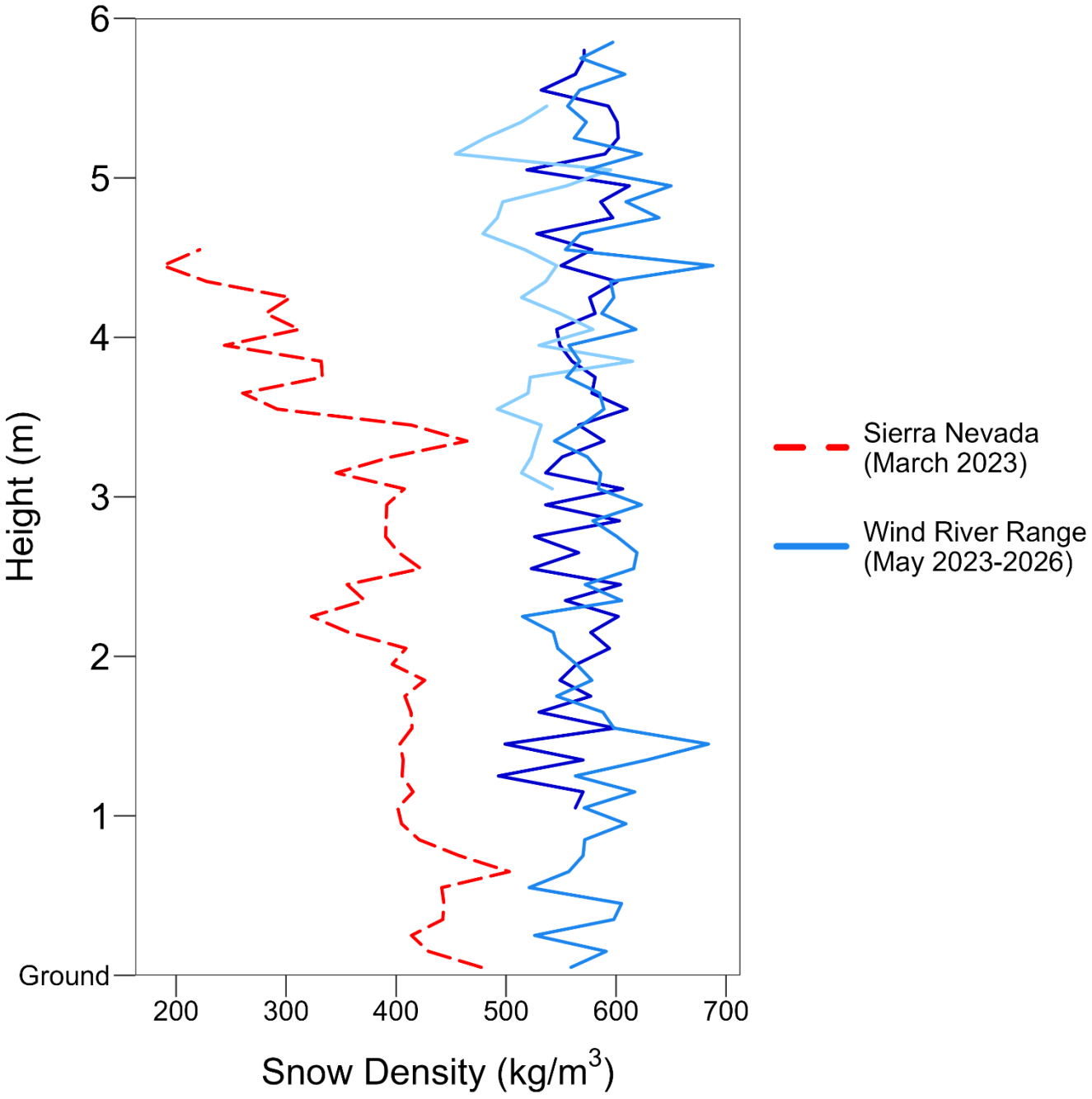

Figure S7: Comparison of deep (> 4 m) snow density profiles between nivation hollow snow drifts in the Wind River Range (late May 2023-2026) and a forested clearing at the Central Sierra Snow Laboratory (CSSL) in the Sierra Nevada (March 11, 2023). Alpine snow drifts have much higher density (mean 526-585 kg/m^{3}compared to 377 kg/m^3) despite comparable depth.